Chinese Chemical Letters 35 (2024) 108955

Contents lists available at ScienceDirect

Chinese Chemical Letters

journal homepage: www.elsevier.com/locate/cclet

Excellent energy storage properties in non-stoichiometric $Bi_{0.5}Na_{0.5}TiO_3$-based relaxor ferroelectric ceramics

Shunshun Jiang[a], Ji Zhang[a,*], Jing Wang[b,*], Shan-Tao Zhang[c]

[a] School of Materials Science and Engineering, Nanjing University of Science & Technology, Nanjing 210094, China
[b] State Key Laboratory of Mechanics and Control of Mechanical Structures, College of Aerospace Engineering, Nanjing University of Aeronautics and Astronautics, Nanjing 210016, China
[c] National Laboratory of Solid State Microstructures, Department of Materials Science and Engineering, College of Engineering and Applied Science & Jiangsu Key Laboratory of Artificial Functional Materials & Collaborative Innovation Center of Advanced Microstructures, Nanjing University, Nanjing 210093, China

ARTICLE INFO

Article history:
Received 27 June 2023
Revised 31 July 2023
Accepted 21 August 2023
Available online 22 August 2023

Keywords:
Non-stoichiometric
$Bi_{0.5}Na_{0.5}TiO_3$
Ceramic capacitor
Energy density
Thermal stability

ABSTRACT

The rapid development of high-power and pulsed-power techniques inspires extensive investigates on high-performance ceramic-based capacitors. However, the low recoverable energy density (W_{rec}) hampers their wider applications. Herein, the non-stoichiometric $Bi_{0.5}Na_{0.5}TiO_3$-based ceramics were designed and studied. The proper introduction of oxygen vacancies facilitated activating defect dipole, giving rise to reduced remanent polarization. Consequently, the optimal composition exhibited an exceptional high W_{rec} of 8.3 J/cm^3, a high efficiency of 85%, and excellent anti-fatigue and thermal reliability. This work provides an efficient approach to explore ceramic capacitors with high capacitive energy storage performances.

Dielectric capacitors with giant power density and ultrafast charge/discharge rate have been popularly used in high-power and pulsed-power electronic devices, including hybrid vehicles, distributed power systems. Yet, the relatively low energy density of dielectric capacitors has become an unavoidable obstacle for the progress of integrated and/or portable devices. Hence, extensive effort has been put in to enhance the energy density of dielectric capacitors for their future applications [1–4].

Among various dielectrics, bismuth sodium titanate ($Bi_{0.5}Na_{0.5}TiO_3$, BNT)-based relaxor ferroelectric ceramics are widely considered as one of up-and-coming materials for capacitive energy storage [1–3,5]. Relaxor ferroelectric ceramics generally possess moderate P_{max} and small P_r induced by polar nanoregions (PNRs) with short-range ferroelectric orders, thus giving rise to moderate W_{rec} (>2 J/cm^3) and high η (> 80%). As for BNT ceramics, the strong hybridization between $6s^2$ lone pair electrons of Bi^{3+} and $2p$ orbitals of O^{2-} triggers a relatively large P_{max} of ~43 μC/cm^2 [6–8]. But the nonergodic relaxor properties of BNT ceramics cause square polarization-electric-field loops (P-E) with large P_r, which seriously hampers the enhancement of energy storage performances [9]. In addition, the Bi^{3+} ions are volatile during sintering under high temperature, leading to the emergence of oxygen vacancies in ceramics. Therefore, the role of oxygen vacancies in the capacitive energy storage properties of BNT-based ceramics still lacks enough research.

Herein, the non-stoichiometric $Sr(Zr_{1/3}Mg_{1/3}Nb_{1/3})O_{3-\delta}$ (SZMN) was incorporated into BNT matrix to generate the oxygen vacancies. The introduction of various ions facilitates disturbing the long-rang ferroelectric orders and promoting the formation of PNRs [1,3]. Additionally, the defect dipole induced by oxygen vacancies contributes to decrease P_r [10]. Consequently, when the applied electric field reached 520 kV/cm, the 0.75BNT-0.25SZMN ceramics exhibited a giant W_{rec} of 8.3 J/cm^3 and a high η of 85%, foreshadowing great prospects in capacitive energy storage.

The (1-x)BNT-xSZMN (x = 0.10, 0.15, 0.20, 0.25, 0.30) ceramics were synthetized by solid state reaction. The crystal structure of (1-x)BNT-xSZMN ceramics was detected by X-ray diffraction (XRD), as displayed in Fig. 1a. The pure perovskite structure for all samples is identified by the typical diffraction peaks, suggesting the introduced dopants have successfully diffused into BNT matrix. The microstructure obtained *via* scanning electron microscope (SEM) are provided in Fig. S1 (Supporting information). All the samples show dense microstructure. With increasing x, the grain size decreases obviously, which is advantageous to achieve high E_b.

Fig. S2 (Supporting information) depict the temperature dependent dielectric constant (ε_r) and loss (tanδ) of (1-x)BNT-xSZMN ce-

* Corresponding authors.
E-mail addresses: jizhang@njust.edu.cn (J. Zhang), wang-jing@nuaa.edu.cn (J. Wang).

https://doi.org/10.1016/j.cclet.2023.108955
1001-8417/

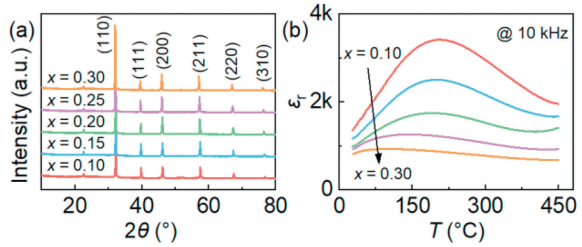

Fig. 1. (a) XRD patterns of (1-*x*)BNT-*x*SZMN ceramics. (b) Temperature dependent ε_r at 10 kHz for $x = 0.10$–0.25.

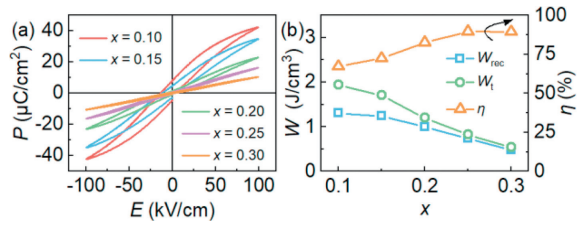

Fig. 2. (a) Bipolar *P-E* loops of (1-*x*)BNT-*x*SZMN ceramics. Composition dependent (b) W_{rec}, W_t, η.

ramics under different frequencies. The wide dielectric peaks, the frequency dependent ε_r, and the increasing T_m (*i.e.*, temperature corresponding to maximum ε_r ($\varepsilon_{r,m}$)) with increasing frequency demonstrate the dielectric relaxor behavior for each sample [6]. Accordingly, the frequency dependent tanδ also confirms the relaxor property. Furthermore, a sharp decrement in tanδ at high temperature is observed, which is ascribed to temperature activated increasing content of defects, such as oxygen vacancies [9]. To better compare the evolution of ε_r for different samples, Fig. 1b plots the composition dependent ε_r at 10 kHz for $x = 0.10$–0.25. Evidently, the dielectric peak becomes more and more wider with increasing x because of the A/B-site disorder and charge fluctuation, implying the improved dielectric realxor behavior. As a result, the ε_r and T_m significantly decrease with increasing x (Fig. 1b). Notably, the temperature insensitive ε_r is highly applicable for high temperature capacitors [6].

Fig. 2a illustrates the composition dependent bipolar *P-E* loops of (1-*x*)BNT-*x*SZMN ceramics at room temperature. The applied electric field and frequency are 100 kV/cm and 10 Hz, respectively. And the corresponding evolution of P_{max}, P_r and P_{max}-P_r is exhibited in Fig. S3 (Supporting information). With increasing x, the *P-E* loop goes slimmer and slimmer, owing to the improved dielectric relaxor behavior. Accordingly, the polarization reduces significantly, especially for P_{max}. This phenomenon is consistent with reduced ε_r (Fig. 1b), because the polarization and dielectric constant show positive relationship [3]. In addition, the concentration of oxygen vacancies, which is confirmed by electron paramagnetic resonance (EPR) spectrum (Fig. S4 in Supporting information), increases by incorporating non-stoichiometric SZMN, giving rise to the emergence of defect dipole. It is well-documented that the defect dipole can construct a built-in electric field, which helps the polarization revert to the initial disorder state [10]. Accordingly, a pinned *P-E* loop with further reduced P_r is observed (Fig. S5 in Supporting information). Owing to the co-contribution of improved relaxor behavior and construction of defect dipole, the P_r of (1-*x*)BNT-*x*SZMN ceramics decreases from 8.0 μC/cm^2 for $x = 0.10$ to 0.5 μC/cm^2 for $x = 0.30$. However, the decrement in P_{max} is larger than that in P_r, resulting in continuous decrement in P_{max}-P_r. Fig. 2b displays the variation of W_{rec}, W_t and η as a function of x. Both W_{rec} and W_t decrease monotonically with increasing x because of the gradual decrement in P_{max} and P_{max}-P_r, while the η increases from 67% for $x = 0.10$ to 89% for $x = 0.30$ owing to successive decrement in P_r.

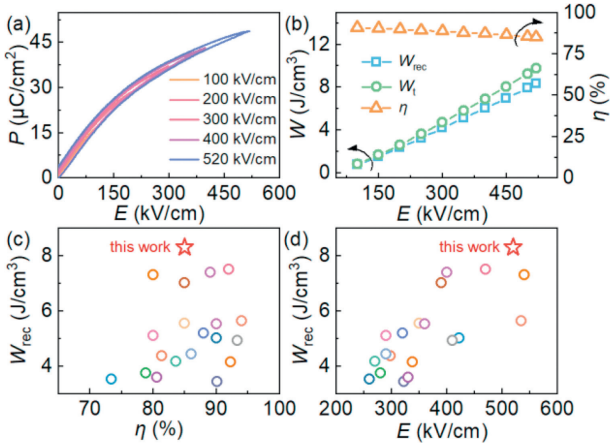

Fig. 3. (a) Electric field dependent unipolar *P-E* loops of the $x = 0.25$ sample, and (b) corresponding W_{rec}, W_t, η. Comparison of (c) W_{rec} and η, and (d) W_{rec} and E between the $x = 0.25$ sample and other BNT-based ceramic capacitors.

Considering the balance between W_{rec} and η, the $x = 0.25$ sample is selected for further investigation.

Fig. 3a exhibits the unipolar *P-E* loops of the $x = 0.25$ sample under different electric fields. And the corresponding electric field dependent P_{max}, P_r and P_{max}-P_r are plotted in Fig. S6 (Supporting information). Under various electric fields, the *P-E* loops always maintain the slim profiles with increased P_{max} and P_r. The P_{max} and P_r of $x = 0.25$ sample reaches 48.9 and 3.7 μC/cm^2 at 520 kV/cm, respectively, leading to the large P_{max}-P_r value of 45.2 μC/cm^2. Nevertheless, the discrepancy between P_{max}-P_r and P_{max} becomes larger and larger (Fig. S6 in Supporting information) owing to the high electric field induced leakage.

Based on the evolution of P_{max}, P_r and P_{max}-P_r, the W_{rec} and W_t of the $x = 0.25$ sample increase monotonically with increasing electric field, while the η gradually decreases, as plotted in Fig. 3b. At the highest applied electric field, the W_{rec}, W_t and η achieve 8.3 J/cm^3, 9.8 J/cm^3 and 85%, respectively. Notably, besides the large value of P_{max}-P_r, the endurance for high electric field up to 520 kV/cm also facilitates obtaining ultrahigh energy density.

To evaluate the superiority in capacitive energy storage, the comparison between the $x = 0.25$ sample and other BNT-based ceramic capacitors is illustrated in Figs. 3c and d [9,11–27]. The detailed information about composition, values of W_{rec}, η and corresponding electric field is listed in Table S1 (Supporting information). It can be seen that the $x = 0.25$ sample achieves the ultrahigh W_{rec} of 8.3 J/cm^3 and high η of 85%, exceeding the most of BNT-based ceramic capacitors, indicating the introduction of proper oxygen vacancies facilitates improving capacitive energy storage performances.

The reliability of capacitive energy storage properties under various conditions is of importance for the practical applications. Fig. 4a shows the cycle number dependent unipolar *P-E* loops of the $x = 0.25$ sample. The applied electric field and frequency is 300 kV/cm and 10 Hz, respectively. When the cycle numbers reach 10^6, the *P-E* loops always remain slim profiles with stable P_{max}, P_r and P_{max}-P_r (Fig. S7 in Supporting information). Accordingly, the W_{rec} and η are 4.1 J/cm^3 and 89% (Fig. 4b), respectively, foreshadowing excellent fatigue behavior. The changeable ambient temperature is inevitable for electronic devices. For example, the operating temperature for the power system of hybrid vehicles can reach as high as 140 °C. The usage of dielectric capacitors with good thermal reliability favors removing extra cooling systems [7,28]. Fig. 4c depicts the unipolar *P-E* loops of the $x = 0.25$ sample in the temperature range of 25–140 °C. The *P-E* loops gradually become fatter with increased P_{max} and P_r (Fig. S7 in Supporting information),

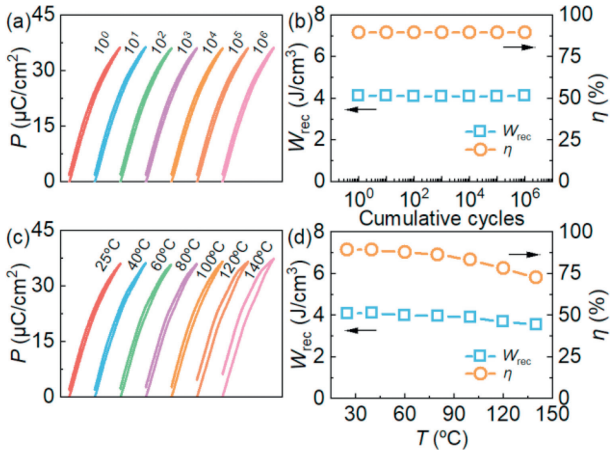

Fig. 4. (a, b) Anti-fatigue and (c, d) thermal reliability of energy storage properties for the $x = 0.25$ sample.

which is scribed to the activation of introduced oxygen vacancies and high temperature induced defects [7]. Consequently, the η decreases from the P_{max}-P_r slightly decreases from 34.1 μC/cm^2 at 25 °C to 31.1 μC/cm^2 at 140 °C because of the simultaneous increment of P_{max} and P_r. Accordingly, the W_{rec} and η decrease from 4.1 J/cm^3 and 89% to 3.5 J/cm^3 and 73% with increasing temperature (Fig. 4d). The variation of W_{rec} and η are 14.6% and 18.0%, indicating promising application in high temperature capacitors. Fig. S8 (Supporting information) plots the comparison of temperature dependent W_{rec} of $x = 0.25$ and other reported BNT-based ceramic capacitors, further suggesting the excellent thermal stability of the $x = 0.25$ sample.

In summary, the non-stoichiometric (1-x)BNT-xSZMN relaxor ferroelectric ceramics were prepared by solid state reaction. The XRD confirmed that the all samples exhibited pure perovskite structure without secondary phase. The temperature dependent ε_r demonstrated the improved dielectric relaxor behavior. The P-E loops went slimmer with reduced P_{max} and P_r due to the synergic effect of dielectric relaxor properties and oxygen vacancies induced defect dipole. Accordingly, an exceptional high W_{rec} of 8.3 J/cm^3 and a high η of 85% were simultaneously achieved in optimal composition of 0.75BNT-0.25SZMN ceramics. Meanwhile, this sample exhibited excellent anti-fatigue (10^0–10^6) and thermal reliability (25–140 °C). These results suggest that the BNT-based ceramic capacitors are superb alternatives for capacitive energy storage.

Declaration of competing interest

The authors declare that they have no known competing financial interests or personal relationships that could have appeared to influence the work reported in this paper.

Acknowledgments

This work was supported by the National Natural Science Foundation of China (Nos. 12004181, 52073144), Natural Science Foundation of Jiangsu Province (Nos. BK20200473, BK20201301) and the Fundamental Research Funds for the Central Universities (No. 30922010309).

Supplementary materials

Supplementary material associated with this article can be found, in the online version, at doi:10.1016/j.cclet.2023.108955.

References

[1] H. Zhang, T. Wei, Q. Zhang, et al., J. Mater. Chem. C 8 (2020) 16648–16667.
[2] F. Zhuo, H. Qiao, J. Zhu, et al., Chin. Chem. Lett. 32 (2021) 2097–2107.
[3] X. Fan, J. Wang, H. Yuan, et al., J. Adv. Ceram. 12 (2023) 649–680.
[4] Z. Sun, J. Zhang, H. Luo, et al., J. Am. Chem. Soc. 145 (2023) 6194–6202.
[5] H. Li, L. Wang, Y. Zhu, P. Jiang, X. Huang, Chin. Chem. Lett. 32 (2021) 2229–2232.
[6] T. Cui, J. Zhang, J. Guo, et al., Acta Mater. 240 (2022) 118286.
[7] H. Wang, J. Zhang, S. Jiang, et al., J. Mater. Chem. A 11 (2023) 4937–4945.
[8] H. Liu, Z. Sun, J. Zhang, et al., J. Am. Chem. Soc. 140 (2023) 11764–11772.
[9] N. Weng, J. Zhang, J. Wang, et al., J. Am. Ceram. Soc. 106 (2023) 2963–2971.
[10] W. Cao, W. Li, Y. Feng, et al., Appl. Phys. Lett. 108 (2016) 202902.
[11] Y.N. Huang, J. Zhang, J. Wang, J. Wang, Y. Wang, J. Mater. Chem. A 11 (2023) 7987–7994.
[12] H. Ji, D. Wang, W. Bao, et al., Energy Storage Mater. 38 (2021) 113–120.
[13] C. Zhang, W. Xiao, F. Zeng, et al., J. Mater. Chem. A 9 (2021) 10088–10094.
[14] F. Yan, K. Huang, T. Jing, et al., Energy Storage Mater. 30 (2020) 392–400.
[15] J. Huang, H. Qi, Y. Gao, et al., Chem. Eng. J. 398 (2020) 125639.
[16] H. Qi, R. Zuo, J. Mater. Chem. A 7 (2019) 3971–3978.
[17] C. Zhu, Z. Cai, B. Luo, et al., ACS Appl. Mater. Interfaces 13 (2021) 28484–28492.
[18] X. Li, X. Dong, F. Wang, et al., J. Eur. Ceram. Soc. 42 (2022) 2221–2229.
[19] D. Li, Y. Lin, Q. Yuan, et al., J. Materiomics 6 (2020) 743–750.
[20] D. Hu, Z. Pan, L. Wu, et al., J. Materiomics 7 (2021) 869–878.
[21] S. Bian, Z. Yue, Y. Shi, J. Zhang, W. Feng, J. Am. Ceram. Soc. 104 (2021) 936–947.
[22] D. Li, D. Zhou, W. Liu, et al., Chem. Eng. J. 419 (2021) 129601.
[23] X. Qiao, A. Sheng, D. Wu, et al., Chem. Eng. J. 408 (2021) 127368.
[24] M. Li, M. Zhu, M. Zheng, et al., J. Mater. Chem. C 10 (2022) 8845–8853.
[25] X. Qiao, F. Zhang, D. Wu, et al., Chem. Eng. J. 388 (2020) 124158.
[26] Y. Chen, Y. Huang, Y. Zuo, et al., J. Eur. Ceram. Soc. 42 (2022) 6985–6996.
[27] W. Shi, L. Zhang, R. Jing, et al., J. Eur. Ceram. Soc. 42 (2022) 4528–4538.
[28] S. Jiang, J. Zhang, J. Wang, et al., Scr. Mater. 235 (2023) 115602.